Dephasing in semiconducting single-walled carbon nanotubes induced by exciton-exciton annihilation

Darius Abramavicius,[1] Ying-Zhong Ma,[2] Matthew W. Graham,[2] Leonas Valkunas,[1] and Graham R. Fleming[2]
[1]*Department of Theoretical Physics, Faculty of Physics of Vilnius University, Sauletekio Avenue 9, Bldg. 3, Vilnius, LT 10222, Lithuania*
and Institute of Physics, Savanoriu 231, Vilnius LT 02300, Lithuania
[2]*Department of Chemistry, University of California, Berkeley,*
and Physical Biosciences Division, Lawrence Berkeley National Laboratory, Berkeley, California 94720-1460, USA
(Received 30 January 2009; revised manuscript received 15 April 2009; published 29 May 2009)

Three-pulse photon echo peak-shift measurements were performed on semiconducting single-walled carbon nanotubes embedded in a polymer matrix at room temperature. We found a striking dependence of the peak shift on the excitation intensity. Numerical simulations based on an interacting-boson model demonstrate that the intensity dependence originates from a highly nonlinear optical response initiated by exciton-exciton annihilation.

DOI: 10.1103/PhysRevB.79.195445 PACS number(s): 78.67.Ch, 71.35.−y, 78.47.jf

I. INTRODUCTION

The optical properties of semiconducting single-walled carbon nanotubes (SWNTs) are governed by excitons with anomalously large binding energies.[1–3] Understanding of exciton dynamics is important from the prospective of both fundamental research and potential applications.[4] Recently, investigations on the coherent phenomena of the excitons have emerged.[5,6] Experiments in the time domain reveal that the dependence of the exciton dephasing rate $(1/T_2)$ on excitation intensity changes markedly with temperature.[6] At 77, 100, and 130 K, a linear dependence on intensity is found, whereas a clear deviation is evident at higher temperature. This deviation indicates possible contributions from inelastic exciton-exciton scattering processes. A significant shortening of exciton population relaxation times T_1 with increasing temperature[7,8] can enhance exciton dephasing at high temperature through the well-known relation $1/T_2=1/T_2^*+1/2T_1$ (T_2^{*-1} is the pure dephasing rate). The results of recent single tube photoluminescence spectroscopy lend support to this inference, where a nonlinear dependence of homogeneous linewidth on excitation intensity was observed and attributed to exciton-exciton annihilation.[5]

To unambiguously identify the effect of population relaxation on exciton dephasing, we employ time-integrated three-pulse photon echo peak-shift (3PEPS) spectroscopy,[9] which is capable of detecting simultaneously exciton dephasing and population relaxation. A key distinction of this incisive tool from conventional two-pulse photon echo or, equivalently, two-pulse degenerate four-wave mixing spectroscopy is the presence of a population period. It offers the capability of elucidating directly the electronic dephasing induced by population transfer processes within the bandwidth of employed laser pulses. We present 3PEPS data for selected semiconducting SWNTs embedded in a solid polymer film. Surprisingly, we find a strong dependence of the photon echo peak shift on excitation intensity, which increases approximately exponentially with decreasing intensity. Note that previous intensive studies on molecules, molecular complexes and aggregates, and polymeric systems have shown that the peak shift is highly insensitive to the processes taking population out of the laser bandwidth.[9]

To identify the origin of this striking intensity dependence, we carried out theoretical model simulations. Third-order nonlinear response theory predicts that a plot of the peak shift as a function of population time T follows closely the correlation function of transition energy fluctuation[10,11] and its signal amplitude is proportional to the cube of excitation intensity. The strong dependence on the intensity observed in this study thus goes beyond the third-order nonlinearity. We use a mean-field approximation (MFA) combined with nonperturbative numerical simulations to convert a complex many-exciton problem into a single-exciton problem and most importantly to calculate the contributions of induced polarizations beyond the usual third-order response. By extracting up to the tenth-order contributions, we show that the exciton-exciton annihilation process contributes substantially to the observed intensity-dependent photon echo peak shift.[12]

II. EXPERIMENT

A commercial D_2O solution of the CoMoCAT nanotubes wrapped with surfactant sodium dodecylbenzene sulfonate was used to fabricate a thin SWNT-polyvinylpyrrolidone (PVP) (SWNT-PVP) composite film of ~200 μm thickness. Use of this solid sample enables significant suppression of the light scattering arising from the motion of nanotubes in the solution sample. A dichloroethane solution of laser dye IR26 was used for reference measurements, which was circulated through a 200-μm-thickness flow cell with a peristaltic pump.

The 3PEPS technique employed here has been described extensively elsewhere.[13] In short, the light source was an optical parametric amplifier pumped by a 250 kHz Ti:Sapphire regenerative amplifier, generating 62 fs pulses at 1018 nm. This wavelength was chosen in order to excite resonantly the lowest transition-allowed excitonic state (E_{11}) of the dominant semiconducting species, the (6,5) tube. The laser beam was split into three replicas of equal intensity

 ©2009 The American Physical Society

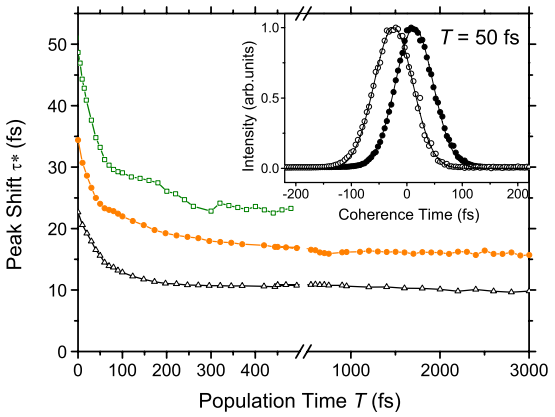

FIG. 1. (Color online) 3PEPS data obtained at three excitation intensities: 3.3 (square), 16.4 (circles), and 92.4 $\mu J/cm^2$ (triangles). The inset shows the normalized time-integrated photon echo profiles collected in the two phase-matching directions $\boldsymbol{k_1}-\boldsymbol{k_2}+\boldsymbol{k_3}$ (open circles) and $-\boldsymbol{k_1}+\boldsymbol{k_2}+\boldsymbol{k_3}$ (filled circles) for the population time $T=50$ fs and an excitation intensity of 18.9 $\mu J/cm^2$. The solid lines are the fits to Gaussian functions.

with wave vectors $\boldsymbol{k_1}$, $\boldsymbol{k_2}$, and $\boldsymbol{k_3}$, and focused to the sample by a 15-cm-focal-length singlet lens. Time-integrated photon echo signals at the two phase-matching directions $\boldsymbol{k_1}-\boldsymbol{k_2}+\boldsymbol{k_3}$ and $-\boldsymbol{k_1}+\boldsymbol{k_2}+\boldsymbol{k_3}$ were detected simultaneously with two InGaAs photodiodes connected to separate lock-in amplifiers.

Representative time-integrated photon echo profiles collected in the two phase-matching directions for a population time $T=50$ fs are plotted as a function of coherence time τ in the inset of Fig. 1. The peak shift at each T is obtained by calculating half the difference between their maxima. The 3PEPS data collected at three different excitation intensities are plotted in Fig. 1 as a function of T. The most intriguing feature of the data is that the peak shift $\tau^*(T)$ strongly depends on excitation intensity. For a given T, an increase in the intensity leads to an approximately exponential decrease of $\tau^*(T)$. This dependence is illustrated in Fig. 2(a) through the peak shift measured at $T=0$. By contrast, the data obtained from a IR26 solution [filled circles in Fig. 2(a)] shows a very small increase (<4 fs) in accord with third-order nonlinear response theory.

Figure 2(b) compares the dependence of the peak amplitude on intensity for SWNTs and IR26. The latter exhibits the expected cubic dependence, whereas the former saturates at very low intensity. A similar saturation behavior was also observed previously for the amplitude of the pump-probe signal and was identified unambiguously as originating from exciton-exciton annihilation.[12] Clearly, the photon echo signal from the SWNTs is no longer governed by the third-order-induced polarization and thus higher-order contributions must be taken into account in order to adequately simulate the unusual intensity-dependent peak-shift data.

III. SIMULATIONS

Theoretical description of the correlations of multiple excitons in semiconductors is a challenging many-body problem.[14,15] At the third order in the field, the description of a two-exciton scattering process must account for not only the Coulomb interactions between the electrons and holes but also their Pauli exclusion.

The simplest tight-binding model Hamiltonian of electrons and holes in a semiconductor (no phonons) in real space is[16]

$$\hat{H} = \sum_i [\varepsilon_i^{(c)} \hat{c}_i^\dagger \hat{c}_i + \varepsilon_i^{(d)} \hat{d}_i^\dagger \hat{d}_i] + \sum_{ij}^{i\neq j} [V_{ij}^{(c)} \hat{c}_i^\dagger \hat{c}_j + V_{ij}^{(d)} \hat{d}_i^\dagger \hat{d}_j] + \sum_{ij} \left[\frac{1}{2} W_{ij}^{(cc)} \hat{c}_i^\dagger \hat{c}_j^\dagger \hat{c}_j \hat{c}_i + \frac{1}{2} W_{ij}^{(dd)} \hat{d}_i^\dagger \hat{d}_j^\dagger \hat{d}_j \hat{d}_i - W_{ij}^{(cd)} \hat{c}_i^\dagger \hat{d}_j^\dagger \hat{d}_j \hat{c}_i \right]. \quad (1)$$

Here $\hat{c}_i^\dagger$ is an electron-creation operator at site i, $\hat{d}_i^\dagger$ is a hole-creation operator, and the operators without daggers are the conjugate annihilation operators. The electron on-site energies are $\varepsilon_i^{(c)}$ while those of holes are $\varepsilon_i^{(d)}$. Electron- and hole-hopping parameters are $V_{ij}^{(c)}$ and $V_{ij}^{(d)}$, respectively. These parameters characterize noninteracting electrons and holes. The rest of the parameters are the Coulomb monopole-monopole interation energies: $W_{ij}^{(cc)}$ between two electrons on sites i and j, $W_{ij}^{(dd)}$ between two holes, and $W_{ij}^{(cd)}$ between an electron and a hole. This Hamiltonian neglects exchange and four-point Coulomb integrals, however it captures the main exciton properties. The electrons and holes are fermions with nonzero anticommutators

$$\hat{c}_i \hat{c}_j^\dagger + \hat{c}_j^\dagger \hat{c}_i = \delta_{ij}, \quad (2)$$

$$\hat{d}_i \hat{d}_j^\dagger + \hat{d}_j^\dagger \hat{d}_i = \delta_{ij}. \quad (3)$$

This Hamiltonian has been used to derive equations of motion for electrons and holes in semiconductors, where each atom is taken as a site. A hierarchy of equations of motion for electron and hole variables are obtained using the Heisenberg equation of motion. The hierarchy is truncated exactly at four-particle correlation functions when considering third-order nonlinear-optical signals. In this case, only two electron-hole pairs need to be considered. Such an approach has been successfully used for semiconductors with the Hamiltonian parameters obtained from *ab initio* simulations.[14,17,18]

The nonlinear behavior of the final equations of motion originate from two sources: the Coulomb interaction and the Pauli exclusion resulting from the Fermion-commutation relations. Instead of using the Fermion-particle-commutation relations for deriving equations of motion, the Pauli-exclusion requirements in real space may be mapped into the nonlinear-interaction potential of bosons as basic particles. While the boson-commutation relations allow the existence of unphysical states, where two electrons (or two holes) as bosons may occupy the same state, such states may be excluded later by forcing their energies out of physical detection window, e.g., to infinity. The anharmonic potential containing such divergencies is then solely responsible for nonlinear signals.

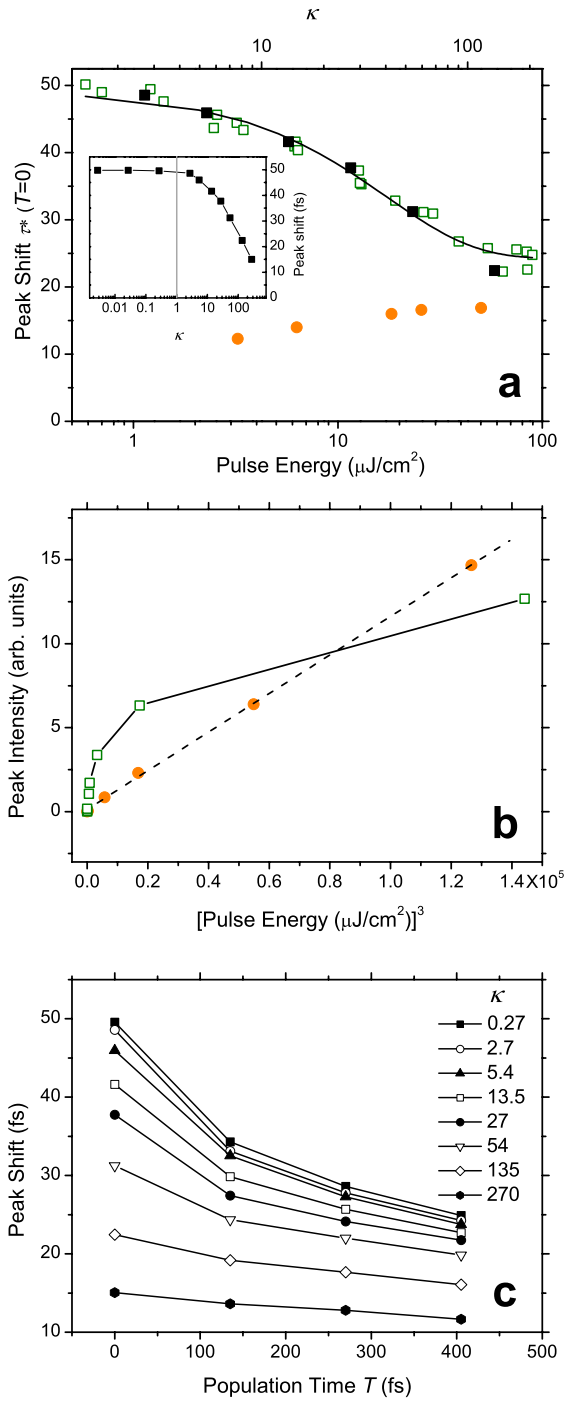

FIG. 2. (Color online) (a) The intensity dependence of the peak shifts at $T=0$ fs obtained for the SWNT-PVP film (open squares) and the IR26 solution (filled circles). The solid line is a monoexponential fit. Filled squares are the simulated result as a function of κ depicted by the scale on the top of the plot (see text). This simulated result is also shown in the inset for a broad range of κ values, and the vertical gray line is drawn for $\kappa=1$, which separates the two intensity regimes. (b) Plot of the corresponding peak amplitudes of the time-integrated photon echo signals versus the cube of the excitation pulse energy. The dotted line is a linear fit to the IR26 data (filled circles), whereas the solid line through the SWNT data (open squares) is drawn to guide the eyes. (c) Simulated 3PEPS decays at different intensities using Eq. (6). The solid lines connecting the symbols are for visual purposes.

The four-point particle-correlation truncation is approximate for our problem of high excitation intensities because high-order many-body correlations may be important at these conditions. Their inclusion expands the hierarchy of necessary equations and the number of parameters considerably. The 3PEPS signal does not directly reveal the many-body resonances, instead it is most sensitive to various dephasing processes. Therefore instead of a full microscopic model, in this paper we develop a phenomenological model of delocalized interacting bosonic excitons representing exciton bands in momentum k space, as inspired by effective bosonization techniques.[19,20] On the basis of delocalized excitons, we treat the exciton bands as an anharmonic ladder of single-exciton, two-exciton, etc., delocalized exciton bands, which is a sufficient level of sophistication for calculating the 3PEPS signal. The starting point of our modeling is the Hamiltonian of interacting single-type bosons, which are excitons in our case, coupled to a phonon bath and an optical field $E(t)$,

$$\hat{H} = \sum_{mn}^{m\neq n} [\delta_{mn} h_{mm} + h'_{mn}(Q)](\hat{b}^\dagger)^m(\hat{b})^n - \hat{P}E(t) + \hat{H}_B, \quad (4)$$

where $h_{00}\equiv 0$, $\hat{b}^\dagger$ is the exciton creation operator, and $\hat{b}$ is the conjugate annihilation operator ($[\hat{b},\hat{b}^\dagger]=1$). $h_{11}\equiv\varepsilon$ is the energy of a single exciton, $h'_{mn}(Q)$ describes the fluctuations induced by phonon coordinate Q characterized by the bath Hamiltonian $\hat{H}_B$. Higher orders of h determine nonlinear exciton properties such as biexciton binding energies (h_{22}) and resonances, etc. In principle, the h_{mm} parameter may be required for describing nonlinear signals up to mth order in the optical field. For isolated excitons ($h'_{mn}=0$, $E=0$), Hamiltonian (4) conserves the number of particles. Since in the following we consider a resonant optical signal, where the laser is tuned to a single-system resonance, this model of a single-type boson is sufficient to capture essential intensity-related effects. The interaction of the system with the optical field is represented by a polarization operator

$$\hat{P} = \mu(\hat{b}^\dagger + \hat{b}), \quad (5)$$

where μ is the transition dipole.

Response of this system to the optical field is described by using perturbation theory with respect to the optical field. The Heisenberg equation is used to determine time evolution of the polarization operator $i\hbar\dot{\hat{P}}=[\hat{H},\hat{P}]$.[16,21] Since $\langle\hat{P}\rangle$ is proportional to $\langle\hat{b}\rangle$, we obtain the equations of motion for the expectation values of products of operators $\hat{b}$. The lowest-order exciton variable is $b\equiv\langle\hat{b}\rangle$; the induced polarization is then $P=\mu b+$c.c.. System nonlinearities lead to an infinite hierarchy of coupled differential equations. These can be closed at a certain order in the incoming field.[21] In the MFA at the third-order in the field, a single equation is obtained[16,21]

$$\frac{d}{dt}b = -i\left(\varepsilon - i\frac{\gamma}{2}\right)b - i\left(\Delta - i\frac{3}{2}\bar{\gamma}\right)b|b|^2 + i\mu E(t), \quad (6)$$

where $\Delta\equiv h_{22}/2$ is the biexciton-binding energy, γ is the linear exciton decay rate, and $\bar{\gamma}$ represents the nonlinear de-

cay of excitons. These rates can be derived using second-order perturbation theory in the Markovian approximation from the off-diagonal fluctuation parameters h'_{10} and h'_{21}. They are given by the Fermi-Golden rule

$$\gamma = \frac{2\pi}{\hbar}|h'_{10}|^2\rho(\varepsilon), \tag{7}$$

$$\bar{\gamma} = \frac{2\pi}{\hbar}|h'_{21}|^2\rho(\varepsilon+\Delta), \tag{8}$$

where $\rho(\omega)$ represents the bath-spectral density. The term proportional to $\bar{\gamma}$ is cubic in $\hat{b}$ and thus describes the transition from two excitons into a single exciton, i.e., reflects exciton-exciton annihilation.

The optical field in a 3PEPS experiment consists of three Gaussian pulses

$$E(t) = \sum_j \mathcal{E}_j(t-\tau_j)\exp[ik_j r - i\omega_0(t-\tau_j)] + \text{c.c.}, \tag{9}$$

where k_j and τ_j are the wave vector and the central time of pulse j with a Gaussian envelope $\mathcal{E}_j(t-\tau_j)$. We consider the same carrier frequency, resonant to the excitation energy $\omega_0=\varepsilon$. For convenience, it is useful to consider chronologically ordered pulses with $\boldsymbol{k}_1$ first and delayed by times τ (between pulses 1 and 2) and T (between 2 and 3). This set of pulses generates a four-wave-mixing signal characterized by the induced nonlinear polarization $P(t)$. It is given by the expectation value of the polarization operator and its time evolution may be calculated from Eq. (6) for a certain configuration of pulse delay times.

The photon echo signal $P_s(t)$ is detected in the $-\boldsymbol{k}_1+\boldsymbol{k}_2+\boldsymbol{k}_3$ phase-matching direction.[22] We do numerical nonperturbative propagation of Eq. (6) to calculate the induced polarization at strong excitations. However, numerically propagated quantities continuously depend on the excitation intensity and different order phase-matching contributions are entangled. Thus the photon echo contributions up to the tenth order in the field are extracted using the phase cycling,[23,24] which is equivalent to the spacial Fourier transformation. A general procedure to extract a certain phase-matching signal at high excitation intensities is as follows. The 2π interval of a jth pulse phase $\Phi_j=k_j r$ is divided into N points, $\Phi_j=\phi n$, $n=(0,\ldots,N-1)$, with a step $\phi=2\pi/N$; N is the order of the signal at which the phase-matching contributions are extracted exactly. The time evolution of the variable b is calculated for a certain pulse-delay configuration according to Eq. (6) as a function of phases $b(\Phi_3,\Phi_2,\Phi_1)$ of three pulses. The $u\boldsymbol{k}_1+v\boldsymbol{k}_2+w\boldsymbol{k}_3$ phase-matching exciton variable may then be obtained using

$$\bar{b}_{uvw} = \sum_{\Phi_3\Phi_2\Phi_1} b(\Phi_3,\Phi_2,\Phi_1)e^{-iu\Phi_3-iv\Phi_2-iw\Phi_1}. \tag{10}$$

Only homogeneous dephasing is included in Eq. (6) via parameters γ and $\bar{\gamma}$ corresponding to the off-diagonal bath fluctuations. Thus the phase-matched homogeneous photon echo-induced polarization is given by

$$P_h(t) = \mu\bar{b}_{-1,1,1}. \tag{11}$$

Structural fluctuations on various time scales induce motional narrowing (additional homogeneous contribution) and inhomogeneous broadening through *diagonal* Hamiltonian fluctuations h'_{11} (for simplicity we neglect h'_{22} and higher terms). Using the time-correlation functions of these fluctuations, their action is expressed through the line-shape functions $g(t)$ by cumulant expansion techniques.[22] We consider the transition-frequency fluctuations ($\tilde{\varepsilon}\equiv h'_{11}$). They are characterized by Gaussian statistics and the corresponding correlation function is

$$\langle\tilde{\varepsilon}(\tau)\tilde{\varepsilon}(0)\rangle = 2\Gamma\delta(\tau) + \sigma_e^2\exp(-\tau/\tau_c), \tag{12}$$

where $\tau\geqslant 0$. Here Γ and σ_e are the strengths of fast and slow phonon modes, respectively, and τ_c is the correlation time of the slow mode. The line-shape function for this type of fluctuations is[22]

$$g(t) = \Gamma t + (\sigma_e\tau_c)^2[\exp(-t/\tau_c) + t/\tau_c - 1], \tag{13}$$

where for slow modes we use $\tau_c^{-1} \ll k_B T/\hbar$ (high temperature) and $\tau_c\sigma_e \gg 1$ (slow limit). This model for $\tau_c\to\infty$ leads to an absorption linewidth of $\sigma_e\sqrt{8\ln(2)}$. The *third-order*-induced polarization at the $-\boldsymbol{k_1}+\boldsymbol{k_2}+\boldsymbol{k_3}$ phase-matching direction for the real line-shape function may be written in the form[22]

$$P_s(t_4) = P_h(t_4)\exp[-g(t_{21}) - g(t_{43}) + g(t_{32}) - g(t_{42}) - g(t_{31}) + g(t_{41})], \tag{14}$$

where $t_{jj'}=t_j-t_{j'}$ are the delays between time-ordered pulses with t_4 standing for the signal-detection time. P_h and P_s are the homogeneous and inhomogeneous signals, respectively. In our simulations, even though they go beyond third-order theory, we use Eq. (14) on top of the homogeneous signal extracted using Eq. (11) to account for diagonal fluctuations.

The photon echo signal in the 3PEPS spectroscopy is a time-integrated intensity at a certain pulse-delay configuration

$$I_s(T,\tau) = \int dt_4|P_s(t_4)|^2. \tag{15}$$

This is simulated for a grid of T and τ values and the peak shift is extracted by the value of τ, where $I_s(T,\tau)$ has its maximum amplitude, as a function of T. In our simulations, the maximum τ value is determined using a parabolic interpolation procedure.

We choose the fundamental transition frequency $\varepsilon = 9800\ \text{cm}^{-1}$, and the parameter Δ, which characterizes the shift of the two-exciton resonances from ε, is set to zero by assuming that the exciton-binding effect in 3PEPS signal is a secondary effect compared to exciton annihilation at high exciton intensities. The dephasing parameter γ and the annihilation parameter $\bar{\gamma}$ are set to $\gamma/\varepsilon = 5.4\times10^{-5}$ (10 ps) and $\bar{\gamma}/\varepsilon = 6.75\times10^{-4}$ (800 fs),[25] respectively, and the inhomogeneous linewidth is chosen to be $\sigma_e/\varepsilon = 0.02$. The diagonal-fluctuation parameters τ_c and Γ were tuned to best reproduce the experimental data $\tau_c\varepsilon = 4000$ and $\Gamma/\varepsilon = 4.5\times10^{-3}$.

The annihilation rate $\bar{\gamma}$ controls the system susceptibility to different excitation intensities [see Eq. (6)]. When the ratio $\bar{\gamma}|b|^2/\gamma \ll 1$, the linear decay dominates. The annihilation is the main relaxation pathway in the opposite limit. This ratio can be estimated by linear-response theory, which gives the maximum $|b^{(1)}|=\mu\bar{\mathcal{E}}$, where $\bar{\mathcal{E}}=\int d\tau \mathcal{E}(\tau)$ is the time-integrated field amplitude. In the presence of diagonal fluctuations, we approximate the polarization decay by σ_e which is usually much larger than γ and introduce an intensity parameter

$$\kappa = \frac{\bar{\gamma}}{\sigma_e}\mu^2\bar{\mathcal{E}}^2. \tag{16}$$

The regime where exciton annihilation becomes important is uniquely defined by the excitation intensity and the ratio of the annihilation rate to the full linewidth.

In the inset of Fig. 2(a), we present the calculated dependence of initial peak shift at $T=0$ on the pulse intensity κ (black squares). It clearly shows the transition behavior from an intensity-independent regime $\kappa \ll 1$ into a regime where the peak shift rapidly decreases when $\kappa \gg 1$. The same calculated values are also plotted in Fig. 2(a) for a narrower range of κ values (from 1.2 to 230), showing very good agreement with experiment. Note that this comparison allows an estimate of the degree of system excitation in the experiment. The calculated 3PEPS decays at different intensities are shown in Fig. 2(c). These decays describe the trend of the observed intensity dependence rather well.

IV. DISCUSSION

The experimental data demonstrate an unusual and striking effect of excitation intensity on photon echo peak shift. Our simulations capture the main feature of the experimental findings—the intensity dependence of peak shift—and also offer insights into the physical mechanism underlying this unusual phenomenon. In our model [Eq. (6)] we have assumed that at high excitation intensities the lifetime-induced dephasing is faster than fluctuation-induced "pure" dephasing. We thus neglect energy exchange with other-band excitons. Equation (14) brings in the contribution of system-bath coupling (fluctuations) to the pure dephasing but does not influence the populations. Thus the combination of the two expressions describes both population dynamics and medium-induced dephasing. With current level of simplifications, our simulations still cannot satisfactorily reproduce the decay behavior of the 3PEPS traces [compare the results shown in Figs. 1 and 2(c)]. To improve the match between the experimental data and simulated results, it may be important to consider a full atomistic model of the nanotube. The simplifications we used include (i) the MFA (no biexciton resonances[26]), (ii) the neglect of multiple exciton-scattering pathways by electrons or holes or excitons beyond phonon-induced annihilation, and (iii) the phenomenological spectral-broadening scheme. However, since the 3PEPS (unlike pump-probe or two-dimensional photon echo) does not directly resolve the many-body resonances but instead reveals dephasing processes, the phenomenological interacting-boson model built directly for delocalized excitons is adequate to explain our 3PEPS data and the physical phenomena behind them. The qualitative agreement between our simulations and the experimental results demonstrate that at high excitation intensities the system behaves as a simple nonlinearly damped oscillator.

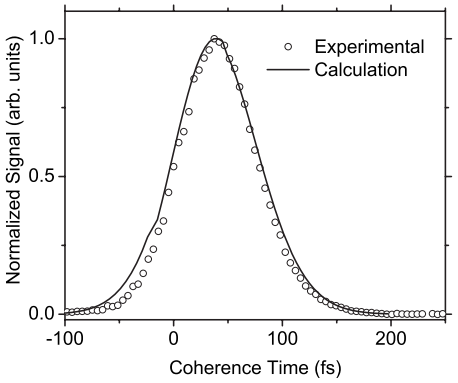

FIG. 3. Measured (symbols) and simulated (line) two-pulse photon echo profiles. The measured data were taken from Fig. 5 of Ref. 27, where a full account of the experimental details can be found. The calculated data were horizontally shifted by −15 fs to account the effect of finite-excitation intensity used to collect the experimental data.

The correlation time of slow bath fluctuations $\tau_c = 2253$ fs determined here is about one order of magnitude longer than the time scale ($\tau_e = 200$) extracted from our previous simulations for an exponential decay term in the correlation function $M(t)$.[27] This difference, at first glance, seems to indicate inconsistency between our previous and current work. However, direct comparison of these time scales is inappropriate because the forms of the correlation functions used are different [compare Eq. (12) above with Eq. 2 in Ref. 27]. Instead, consistency between our previous and current simulations is verified through calculations of both 3PEPS and two-pulse photon echo signals using these $M(t)$ functions and confirmed by the similar results for both cases (data not shown). We further find that the correlation function given by Eq. (12) can reproduce very well the decay behavior of an experimental two-pulse photon echo profile acquired using a similar SWNT-PVP film (see Fig. 3). This long τ_c-time scale accounts for both the slow bath fluctuations and the peak-shift offset at population times longer than ≈300 fs (see Fig. 1). This offset was modeled by an additional term describing static inhomogenity in our previous paper.[27] The present correlation function thus constitutes the simplest model, which agrees approximately with the 3PEPS data.

The remarkable intensity dependence of the photon echo peak shift sets SWNTs apart from almost all other systems studied by this technique to date. Although a decrease in the photon echo peak shift with increasing excitation intensity was reported by Cundiff and co-workers[28] for GaAs quantum wells, no analysis was presented and therefore the cause leading to the observed dependence remains unknown. The strong dependence of the initial peak-shift value [Figs. 1 and 2(a)], the absence of a dependence on population time,[27] and the marked derivation from the typically observed cubic de-

pendence on excitation intensity [Fig. 2(b)] found from the semiconducting SWNTs all imply the existence of a dephasing mechanism dependent on the creation of multiple excitons.

According to our simulations, the observed intensity dependence of peak shift arises from two levels of electronic dephasing—a characteristic intensity-independent dephasing of single exciton and an intensity-dependent dephasing owing to an enhanced exciton-exciton scattering in this spatially confined system.[6] These dephasing processes are described in our simulations by the dephasing parameter γ and the pulse intensity parameter κ, respectively. Since we let $\Delta=0$ in our simulations, we find that exciton-exciton annihilation makes a major contribution to the intensity dependence compared to other possible elastic and inelastic exciton-exciton scattering pathways.

ACKNOWLEDGMENTS

The work at Berkeley was supported by the NSF. D.A. and L.V. acknowledge the Lithuanian State Science and Studies Foundation for financial support.

[1] F. Wang, G. Dukovic, L. E. Brus, and T. F. Heinz, Science **308**, 838 (2005).
[2] J. Maultzsch, R. Pomraenke, S. Reich, E. Chang, D. Prezzi, A. Ruini, E. Molinari, M. S. Strano, C. Thomsen, C. Lienau, Phys. Rev. B **72**, 241402(R) (2005).
[3] Y.-Z. Ma, L. Valkunas, S. M. Bachilo, and G. R. Fleming, J. Phys. Chem. B **109**, 15671 (2005).
[4] Y.-Z. Ma, T. Hertel, Z. V. Vardeny, G. R. Fleming, and L. Valkunas, in *Carbon Nanotubes*, Topics in Applied Physics, edited by A. Jorio, G. Dresselhaus, and M. S. Dresselhaus (Springer-Verlag, Berlin, Heidelberg, 2008), Vol. 111, p. 321.
[5] K. Matsuda, T. Inoue, Y. Murakami, S. Maruyama, and Y. Kanemitsu, Phys. Rev. B **77**, 033406 (2008).
[6] Y.-Z. Ma, M. W. Graham, G. R. Fleming, A. A. Green, and M. C. Hersam, Phys. Rev. Lett. **101**, 217402 (2008).
[7] Y.-Z. Ma, L. Valkunas, S. M. Bachilo, and G. R. Fleming, Phys. Chem. Chem. Phys. **8**, 5689 (2006).
[8] S. Berger, C. Voisin, G. Cassabois, C. Delalande, P. Roussignol, and X. Marie, Nano Lett. **7**, 398 (2007).
[9] G. R. Fleming, S. A. Passino, and Y. Nagasawa, Philos. Trans. R. Soc. London, Ser. A **356**, 389 (1998).
[10] G. R. Fleming, T. Joo, and M. Cho, Adv. Chem. Phys. **101**, 141 (1997).
[11] M. Cho, J.-Y. Yu, T. Joo, Y. Nagasawa, S. A. Passino, and G. R. Fleming, J. Phys. Chem. **100**, 11944 (1996).
[12] Y.-Z. Ma, L. Valkunas, S. L. Dexheimer, S. M. Bachilo, and G. R. Fleming, Phys. Rev. Lett. **94**, 157402 (2005).
[13] T. Joo, Y. Jia, J.-Y. Yu, M. J. Lang, and G. R. Fleming, J. Chem. Phys. **104**, 6089 (1996).
[14] V. M. Axt and S. Mukamel, Rev. Mod. Phys. **70**, 145 (1998).
[15] H. Huag and S. W. Koch, *Quantum Theory of the Optical and Electronic Properties of Semiconductors*, 4th ed. (World Scientific, Singapore, 2004).
[16] R. Oszwaldowski, D. Abramavicius, and S. Mukamel, J. Phys.: Condens. Matter **20**, 045206 (2008).
[17] G. Khitrova, H. M. Gibbs, F. Jahnke, M. Kira, and S. W. Koch, Rev. Mod. Phys. **71**, 1591 (1999).
[18] R. Oszwałdowski, M. Reichelt, T. Meier, S. W. Koch, and M. Rohlfing, Phys. Rev. B **71**, 235324 (2005).
[19] A. O. Gogolin, A. A. Nersesyan, and A. M. Tsvelik, *Bosonization and Strongly Correlated Systems* (Cambridge University Press, Cambridge, UK, 1998).
[20] S. Okumura and T. Ogawa, Phys. Rev. B **65**, 035105 (2001).
[21] V. Chernyak, W. M. Zhang, and S. Mukamel, J. Chem. Phys. **109**, 9587 (1998).
[22] S. Mukamel, *Principles of Nonlinear Optical Spectrscopy* (Oxford University Press, New York, 1995).
[23] P. Tian, D. Keusters, Y. Suzaki, and W. S. Warren, Science **300**, 1553 (2003).
[24] T. Mancal, A. V. Pisliakov, and G. R. Fleming, J. Chem. Phys. **124**, 234504 (2006).
[25] F. Wang, G. Dukovic, E. Knoesel, L. E. Brus, and T. F. Heinz, Phys. Rev. B **70**, 241403(R) (2004).
[26] M. R. Salvador, P. S. Nair, M. Cho, and G. D. Scholes, Chem. Phys. **350**, 56 (2008).
[27] M. W. Graham, Y.-Z. Ma, and G. R. Fleming, Nano Lett. **8**, 3936 (2008).
[28] S. G. Carter, Z. Chen, and S. T. Cundiff, Phys. Rev. B **76**, 121303(R) (2007).